Analyst

PAPER

Cite this: *Analyst*, 2015, **140**, 2869

Electrokinetic preconcentration of particles and cells in microfluidic reservoirs†

Herbert Harrison,[a] Xinyu Lu,[a] Saurin Patel,[a] Cory Thomas,[a] Andrew Todd,[a] Mark Johnson,[a] Yash Raval,[b] Tzuen-Rong Tzeng,[b] Yongxin Song,[c] Junsheng Wang,[d] Dongqing Li[e] and Xiangchun Xuan*[a]

Received 18th January 2015,
Accepted 23rd February 2015

DOI: 10.1039/c5an00105f

www.rsc.org/analyst

Preconcentrating samples of dilute particles or cells to a detectable level is required in many chemical, environmental and biomedical applications. A variety of force fields have thus far been demonstrated to capture and accumulate particles and cells in microfluidic devices, which, however, all take place within the region of microchannels and may potentially cause channel clogging. This work presents a new method for the electrokinetic preconcentration of 1 μm-diameter polystyrene particles and *E. coli* cells in a very-low-conductivity medium inside a microfluidic reservoir. The entire microchannel can hence be saved for a post-concentration analysis. This method exploits the strong recirculating flows of induced-charge electroosmosis to concentrate particles and cells near the corners of the reservoir–microchannel interface. Positive dielectrophoresis is found to also play a role when small microchannels are used at high electric fields. Such an in-reservoir electrokinetic preconcentration method can be easily implemented in a parallel mode to increase the flow throughput, which may potentially be used to preconcentrate bacterial pathogens in water.

Introduction

Preconcentrating samples of dilute particles or cells to a detectable level for subsequent analysis such as enzyme-linked immunosorbent assay (ELISA) and polymerase chain reaction (PCR) is critical in many chemical, environmental and biomedical applications such as food industry, water treatment, disease diagnostics *etc*.[1–3] Microfluidic devices have been increasingly used in the past two decades to trap and enrich diverse particles and cells due to their capability for more precise control over macroscopic counterparts and their potential for parallel operation for high throughput without compromising the efficiency.[4,5] Numerous microfluidic techniques have thus far been developed to concentrate particles, among which contactless methods are often preferred over surface-contact methods.[6,7] In the latter case, mechanical blocking and chemical bonding are the two frequently used approaches to immobilize and accumulate particles and cells onto engineered surfaces, which, though straightforward, usually suffer from the issues of irreversible adhesions and device fouling.[8–10] In contrast, contactless methods utilize an externally applied force field to remotely capture and enrich particles and cells in either a flowing or a stationary suspension. These types of methods offer the flexibility of reversible trapping and as well easy control of the trapping position *via* simply turning on and off the force field at a custom-designed location.[6,7]

A variety of non-electrical forces including acoustic,[11–14] magnetic[15–18] and optical[19–22] fields have been demonstrated to trap and concentrate particles and cells without contact in microfluidic devices. Compared to these methods, electric field-driven particle and cell enrichment is simpler to implement and reconfigure into lab-on-a-chip devices due to the ease of electrical connection and integration.[23–25] To date electrokinetic contactless preconcentration of particles and cells in microfluidic devices has been implemented by primarily four different means. In the first means, a nanoporous membrane is integrated into one microchannel[26] or between two microchannels,[27] through which the electrokinetic preconcentration of particles and cells can be achieved *via* ion concentration polarization. The second means uses a pressure-driven flow to oppose electroosmotic fluid flow in a microchannel with multiple converging and diverging elements

[a]*Department of Mechanical Engineering, Clemson University, Clemson, SC 29634-0921, USA. E-mail: xcxuan@clemson.edu; Fax: +864-656-7299*
[b]*Department of Biological Sciences, Clemson University, Clemson, SC 29634-0314, USA*
[c]*College of Marine Engineering, Dalian Maritime University, Dalian 116026, China*
[d]*College of Information Science and Technology, Dalian Maritime University, Dalian 116026, China*
[e]*Department of Mechanical and Mechatronics Engineering, University of Waterloo, Waterloo, ON N2L 3G1, Canada*
†Electronic supplementary information (ESI) available. See DOI: 10.1039/c5an00105f

where recirculating flows can be generated to concentrate particles.[28] The third means utilizes the recirculating fluid flows that arise from the polarization of electrode (*i.e.*, ac electroosmosis)[29–31] or dielectric (*i.e.*, induced-charge electroosmosis or ICEO[32] in short)[33–35] surfaces or the inevitable Joule heating effects (*i.e.*, electrothermal flow)[36,37] in electrokinetics to concentrate particles and cells. The fourth means, which is also the most often used approach, makes use of particle dielectrophoresis (DEP) that is induced by the gradients in an externally imposed dc and/or ac electric field.[38,39] Electric field non-uniformity can be created by an array of microelectrodes[40–42] and/or micro-insulators (*e.g.*, hurdles and posts)[43–52] that are patterned inside microchannels.

However, particle and cell preconcentrations in the above-reviewed methods have all been restricted to take place inside microchannels. This may cause a potential clogging of the microchannels due to the limited space therein and in turn the fouling of the microfluidic devices. Therefore, our group has recently developed a new approach that can continuously trap and enrich particles and cells inside the inlet reservoir that is far larger in volume than a microchannel.[53,54] The probability of channel fouling is greatly reduced, and more importantly, the entire microchannel can be saved for post-concentration analysis. Our approach exploits the negative dielectrophoretic motion of particles, which is induced by the inherent electric field gradients at the reservoir–microchannel junction, to counterbalance the electrokinetic flow for particle trapping.[55] Since particles need to be suspended in a more conductive medium, this approach may suffer from Joule heating effects when working with small particles at high electric fields.[56] In this work we present for the first time an in-reservoir electrokinetic particle preconcentration in a very dilute medium *via* the combined action of ICEO and positive DEP. Due to the extremely low electric conductivity of the suspending medium, Joule heating is no longer an issue. The application of this trapping approach to *E. coli* cells is demonstrated.

Experiment

Fabrication of microchannels

Fig. 1 shows a picture of the microfluidic chip used in the experiment, which was fabricated with polydimethylsiloxane (PDMS) *via* the standard soft lithography technique. The detailed fabrication process is presented elsewhere.[53] The straight channel is 3.3 mm long with a reservoir at each end and is 25 μm deep everywhere. It is 500 μm wide in the main body and abruptly tapers to a 25 μm or 50 μm wide constriction of 180 μm length at the entrance, *i.e.*, the inlet reservoir and microchannel junction as viewed from the inset in Fig. 1. This constriction was designed for the purpose of reducing the magnitude of the applied electric voltage because of the local amplification of electric field. The inlet and outlet reservoirs were both made very large (6 mm in diameter each) in order to reduce the influence of pressure-driven backflow due to the liquid buildup in the outlet reservoir during the course of the experiment.[57]

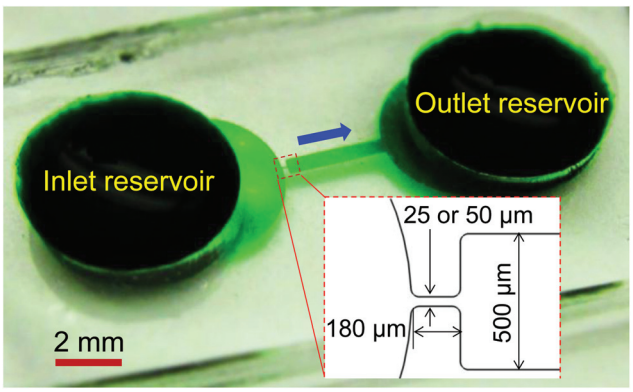

Fig. 1 Picture of the microfluidic chip (the microchannel and reservoirs are filled with green dye for clarity) used in experiments (the block arrow indicates the particle or cell moving direction). Important dimensions of the reservoir–microchannel junction are labeled on the inset, which is also the region of particle visualization.

Preparation of particle and cell suspensions

To implement the in-reservoir electrokinetic preconcentration, polystyrene particles with 1 μm diameter (Polysciences, Warrington, PA) were re-suspended in 0.01 mM phosphate buffer to a final concentration of around 10^7 particles per milliliter. The electric conductivity of this solution was measured (Accumet AP85, Fisher Scientific) to be about 6 μS cm^{-1}. To demonstrate the application in biological cells, *E. coli* ORN208 cells were transformed with green fluorescent protein (gfp)-encoding plasmid pGREEN by electroporation.[58] The transformed bacterial cells were grown in tryptic soy broth (TSB)/tryptic soy agar (TSA) supplemented with ampicillin (50 μg ml^{-1}). For experimental purpose, a single colony of *E. coli* ORN208 was inoculated in TSB media (20 milliliter) for 14–16 hours at 37 °C under shaking conditions (200 rpm). The cells were then centrifuged at 3000*g* for 3 min before being re-suspended in 1× phosphate buffered saline (PBS) solution. After washing the cells thrice, they were finally re-suspended into 0.01 mM phosphate buffer prior to test at an approximate concentration of 10^8 cells per milliliter (based on optical density readings). Tween 20 (0.1% v/v, Sigma-Aldrich) was added to both the particle and cell suspensions to prevent particle per cell aggregations and adhesions to channel walls.

Pumping and imaging of particle and cell suspensions

The pumping of particle and cell suspensions and the in-reservoir preconcentration of particles and cells were implemented simultaneously by the application of a single dc-biased ac electric field across the microchannel. The electric voltages were supplied by a function generator (33220A, Agilent Technologies) and amplified through a high voltage amplifier (609E-6, Trek, Inc.). During the experiment the dc voltage was maintained at 10 V while the ac voltage (fixed at 1 kHz frequency, no more than 300 V in the root-mean-squared magnitude) was

varied to study the electric field effects on electrokinetic particle per cell transport from the inlet reservoir to the microchannel. Joule heating effects were estimated to be negligible in the tested solution under these electric fields, which is reflected by the very small increase in the measured electric current during the experiment.[59] The pressure-driven particle per cell motion was minimized by carefully balancing the liquid volumes in the two reservoirs prior to every test. To further reduce the effects of pressure-driven backflow and ensure a purely electrokinetic transport during the experiment, every test was run for no more than 1 min. The particle and cell behaviors at the reservoir–microchannel junction were observed with an inverted fluorescence microscope (Eclipse TE2000U, Nikon Instruments) and recorded with a CCD camera (Nikon DS-QilMC) at a rate of 15 frames per second. The obtained digital images were post-processed with Nikon imaging software (NIS-ELEMENTS AR 2.30).

Mechanism

Fig. 2 illustrates the particle motions that occur at the reservoir–microchannel junction under the application of an electric field (either dc or dc-biased ac). The background thin lines display the electric field lines, which also represent the fluid streamlines of electrokinetic flow. The electrokinetic velocity, $\mathbf{U}_{EK}$, of a particle is a combination of fluid electroosmosis and particle electrophoresis, both of which are linear functions of the imposed dc electric field, $\mathbf{E}_{dc}$, *via* the interaction with the surface charge (or zeta potential) spontaneously formed on the channel and particle surfaces,[23–25]

$$\mathbf{U}_{EK} = \mu_{EK}\mathbf{E}_{dc} \tag{1}$$

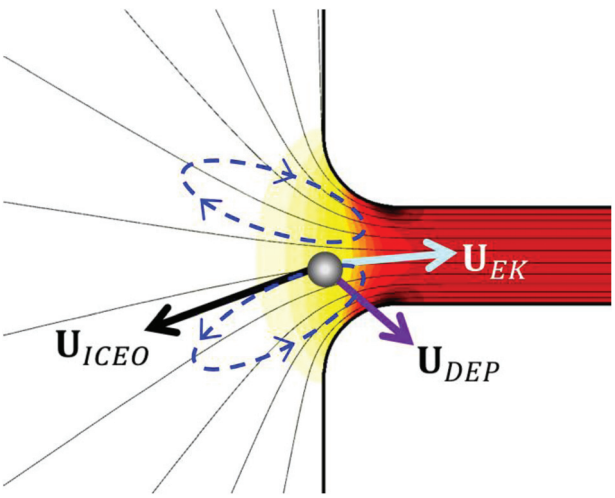

Fig. 2 Schematic illustrating the mechanism of electrokinetic preconcentration of particles and cells at the reservoir–microchannel junction. The symbols $\mathbf{U}_{ICEO}$, $\mathbf{U}_{DEP}$ and $\mathbf{U}_{EK}$ represent the fluid velocity due to induced-charge electroosmosis (ICEO, flow direction is highlighted by the dashed-line arrows), particle velocity due to positive reservoir-based dielectrophoresis (DEP), and electrokinetic particle velocity, respectively. The thin lines represent the electric field lines and the background color shows the contour of electric field squared (the darker the color, the larger the magnitude).

where μ_{EK} is the electrokinetic particle mobility. The application of electric field also induces charges on the channel surface due to the weak polarizability of the PDMS walls,[60,61] especially significant for the two corners at the junction.[62,63] The resulting fluid flow due to the interaction of electric field and induced charges, *i.e.*, induced-charge electroosmosis (ICEO),[32] appears in the form of a pair of counter-rotating vortices with directions being highlighted by dashed-line arrows in Fig. 2. This flow carries particles along with it at a velocity, $\mathbf{U}_{ICEO}$,[32,60]

$$\mathbf{U}_{ICEO} \sim \lambda_D \frac{\varepsilon_w}{\varepsilon_m}\mathbf{E}^2 \tag{2}$$

where λ_D is the Debye screening length which is about 100 nm in 0.01 mM buffer, ε_w and ε_m are the dielectric permittivities of the channel wall and the suspending medium, respectively. Due to a quadratic dependence on the electric field, both the dc and ac field components contribute to $\mathbf{U}_{ICEO}$.

Moreover, as viewed from the contour of $\mathbf{E}^2$ in Fig. 2 (the darker the background color, the larger the magnitude), strong electric field gradients are inherently induced at the junction due to the significant size-mismatch between the reservoir and the microchannel. Therefore as a particle travels through the reservoir–microchannel junction, it experiences a dielectrophoretic force.[55] For rigid spherical particles of diameter d in dc and low-frequency (<100 kHz) ac electric fields, the resulting dielectrophoretic particle velocity, $\mathbf{U}_{DEP}$, is given by[38]

$$\mathbf{U}_{DEP} = \frac{\varepsilon_m d^2 f_{CM}}{12\eta_m}\nabla\mathbf{E}^2 \tag{3}$$

where η_m and σ_m are the dynamic viscosity and electric conductivity of the suspending medium, respectively, and $f_{CM} = (\sigma_p - \sigma_m)/(\sigma_p + 2\sigma_m)$ is the Clausius–Mossotti factor that has been assumed to be approximately equal in dc and low-frequency ac electric fields[25,44–46] with σ_p being the electric conductivity of the particle. When a particle is more conductive than the fluid, *i.e.*, $f_{CM} > 0$, it experiences positive DEP and is pulled towards regions of higher electric field, *i.e.*, the corners of the reservoir–microchannel junction (see both the direction of $\mathbf{U}_{DEP}$ and the contour of $\mathbf{E}^2$ in Fig. 2). In contrast, a particle that is less conductive than the fluid experiences negative DEP (*i.e.*, $f_{CM} < 0$), and is repelled away from the constriction, *i.e.*, against $\mathbf{U}_{EK}$. This function has been demonstrated in our earlier papers to concentrate particles and cells of several microns in diameter,[53–55] which, as noted in the Introduction section, is however prone to Joule heating effects due to the use of a more conductive suspending medium.[56] As we will present in the results section below, the combined action of $\mathbf{U}_{ICEO}$ and positive $\mathbf{U}_{DEP}$, particularly the former due to its much longer working range, enables the in-reservoir electrokinetic preconcentration of particles and cells in very dilute solutions without the concern of Joule heating effects.

Results and discussion

In-reservoir electrokinetic preconcentration of polystyrene particles

Fig. 3 shows the electrokinetic behaviors of 1 μm-diameter polystyrene particles at the reservoir–microchannel junction under the application of various ac electric voltages with a fixed 10 V dc bias. The constricted section of the microchannel (see the inset in Fig. 1) is 25 μm wide. The illustrated top-view snapshot images in Fig. 3 were each taken at 15 s after the respective electric field was switched on. Under a 50 V ac voltage, all particles travel through the constriction without noticeable migrations across fluid streamlines in Fig. 3(A).

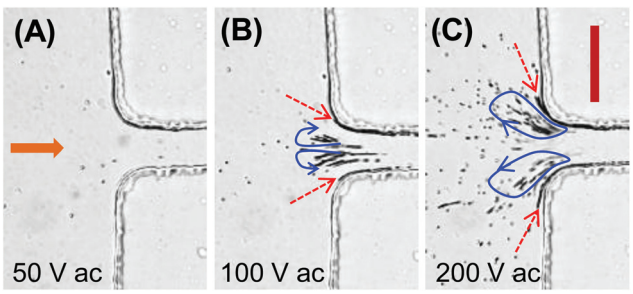

Fig. 3 Top-view snapshot images illustrating the ac electric field effect on electrokinetic transport and trapping of 1 μm polystyrene particles at the reservoir–microchannel (with a 25 μm wide constriction, see Fig. 1) junction: (A) 50 V ac, (B) 100 V ac, (C) 200 V ac. The dc voltage is fixed at 10 V. The dashed-line arrows highlight the trapped particles on the corner surfaces due to positive DEP and the curved-line arrows highlight the particles trapped in the bulk fluid by the recirculating flows of ICEO. The block arrow indicates the particle traveling direction in all cases. The scale bar represents 50 μm.

Under a 100 V ac voltage particles get trapped at the junction in two locations (see Movie 1 in the ESI†). The primary location is in the bulk fluid where particles are concentrated in the form of clusters inside a pair of counter-rotating vortices, which, as highlighted by the curved arrows in Fig. 3(B) (see also Fig. 2), is the typical flow pattern of ICEO.[32,34,35,60,61,63] The secondary location of preconcentration is on the surfaces of the two corners where particles form long chains lining the channel walls as highlighted by the dashed-line arrows in Fig. 3(B). This is a direct evidence of positive DEP[38] (see Fig. 2), which takes place because the particle with σ_p = 40 μS cm^{-1} is more conductive than the suspending medium with σ_m = 6 μS cm^{-1} and hence has a positive CM factor, f_{CM} = 0.65. The particle conductivity was estimated using the formula, $\sigma_p = 4K_s/d$ with K_s = 1 ns being the recommended value for the surface conductance of polystyrene particles.[64] When the ac voltage increases to 200 V, the two fluid vortices become stronger in size and speed due to the dependence of $\mathbf{U}_{ICEO}$ on $\mathbf{E}^2$ in eqn (2). Moreover, the centers of both vortices are shifted towards the adjacent corners (see Movie 2 in the ESI†). Therefore, particles are concentrated in these near-wall vortices, which turn out to also enhance particle trapping by positive DEP on the corner surfaces as demonstrated in Fig. 3(C).

The time development of this in-reservoir electrokinetic particle preconcentration is displayed in Fig. 4 for both 100 V (A) and 200 V (B) ac voltages with a fixed 10 V dc bias. In the first 5 s, particles are trapped by the vortices of ICEO near the center region of the channel entrance under 100 V ac in Fig. 4(A). They first form chains which then extend and interact with each other to form clusters as seen from the image at 10 s. Moreover, the trapping zone expands towards the two corners

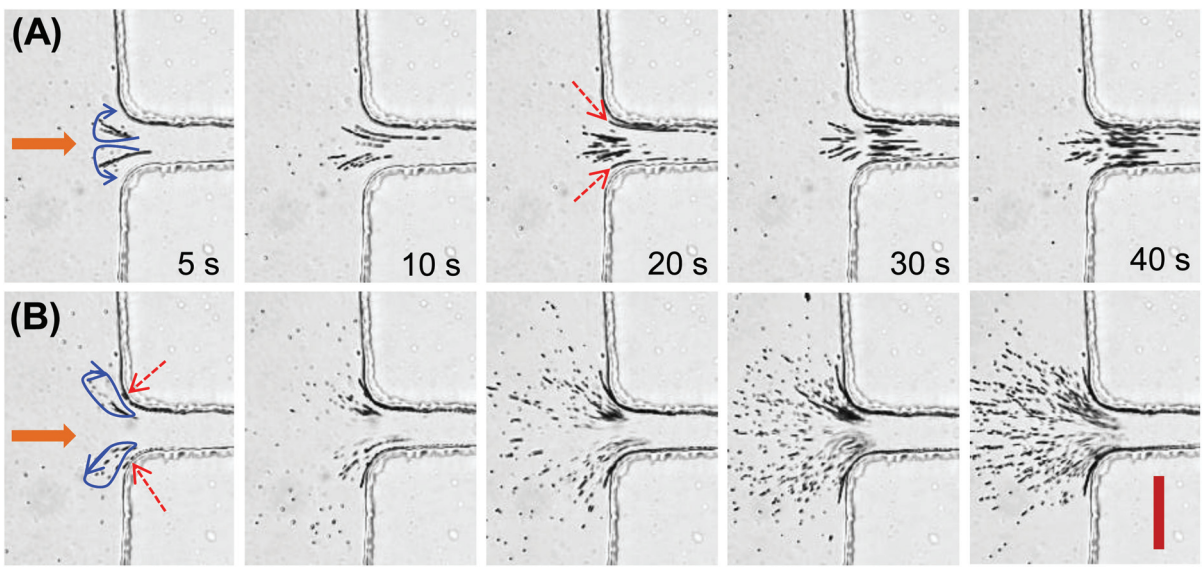

Fig. 4 Time (labeled on the images) development of in-reservoir electrokinetic preconcentration of 1 μm polystyrene particles under 100 V ac (A) and 200 V ac (B). The dc voltage is fixed at 10 V and the constricted section of the microchannel (see Fig. 1) is 25 μm wide. The dashed-line arrows highlight the trapped particles on the corner surfaces due to positive DEP and the curved-line arrows highlight the particles trapped in the bulk fluid by the recirculating flows of ICEO. The block arrows indicate the particle traveling direction. The scale bar represents 50 μm.

where positive DEP takes effect to pull particle chains onto the walls at 20 s. It further extends into the microchannel and spans the entire width with more particles being concentrated at 30 s and 40 s, which may eventually cause a clogging of the channel and thus, should be avoided in applications. In contrast, under 200 V ac both ICEO and positive DEP become strong and act to concentrate particles near the corners of the channel from the beginning of the test as seen from the image at 5 s in Fig. 4(B). Moreover, the trapping zone extends significantly into the reservoir and also over the cross-section of the channel entrance as the particle preconcentration progresses. However, due to the disturbance of ICEO, the trapped particles circulate quickly in the two vortices with few chains or clusters being formed, which indicates the greater impact of ICEO than DEP. Therefore, high ac voltages are preferred in order to preconcentrate particles inside the reservoir and avoid channel clogging.

The preconcentrated particles can be dispersed by turning off either the entire actuation voltage (*i.e.*, both DC and AC components) or the AC voltage component alone. In the former situation, both fluid and particle motions, *i.e.*, $\mathbf{U}_{EK}$, $\mathbf{U}_{ICEO}$, and $\mathbf{U}_{DEP}$ in Fig. 2, are completely stopped. Therefore, the trapped particles get dispersed right at the reservoir and microchannel interface, which may be taken out of the reservoir using a micropipette for out-of-spot analysis. If, however, only the AC voltage component is turned off, the DC voltage-driven $\mathbf{U}_{EK}$ remains unvaried while $\mathbf{U}_{ICEO}$ and $\mathbf{U}_{DEP}$ are both substantially reduced. As a consequence, the vortices if still available become so weak that the preconcentrated particles can no longer be held inside the reservoir and hence are flushed into the microchannel by $\mathbf{U}_{EK}$. The particles are then dispersed in the flow and may be exposed to other forces or chemicals for further analysis inside the microchannel.

Geometric effect on in-reservoir electrokinetic particle preconcentration

Fig. 5 shows the time development of the electrokinetic preconcentration of 1 μm particles at the reservoir–microchannel junction with a 50 μm wide constriction (see the inset in Fig. 1) under a 10 V dc-biased 300 V ac (see Movie 3 in the ESI†). The local electric field squared, $\mathbf{E}^2 = (1 + \alpha^2)\,\mathbf{E}_{dc}^2$ with α = 30 being the ac to dc field ratio, is approximately equal to that inside the 25 μm wide constriction in Fig. 4(B) under a 10 V dc-biased 200 V ac (*i.e.*, α = 20). This is because $\mathbf{E}_{dc}$ in the latter case is about twice that within the 50 μm wide constriction. Therefore, the particle velocity due to ICEO, $\mathbf{U}_{ICEO}$ in eqn (2), remains approximately the same in the two tests in Fig. 4(B) and 5. However, the dielectrophoretic particle velocity, $\mathbf{U}_{DEP}$ in eqn (3), gets weaker in the 50 μm wide constriction due to the decrease in electric field gradients or more accurately $\nabla\mathbf{E}^2$. As a consequence, positive DEP should play an even smaller role in Fig. 5 than in Fig. 4(B). This analysis is supported by the images in Fig. 5 where no particles are observed to be trapped onto the channel walls. Moreover, the zone of particle preconcentration *via* ICEO seems to be further pushed away from the microchannel wherein very few particles are trapped. This may be (partially) attributed to the decrease in both $\mathbf{U}_{EK}$ and positive $\mathbf{U}_{DEP}$ (note that the latter has a streamwise component in the same direction as the former; see Fig. 2) as compared to the corresponding particle velocity components in Fig. 4(B).

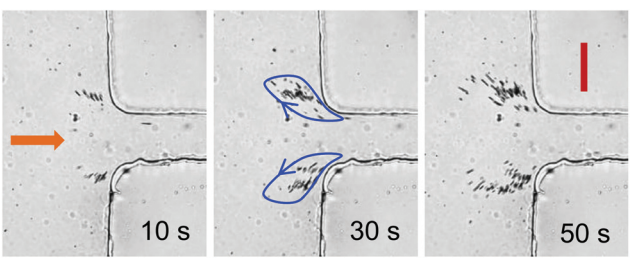

Fig. 5 Time development of electrokinetic preconcentration of 1 μm polystyrene particles at the reservoir–microchannel (with a 50 μm wide constriction, see Fig. 1) junction under the application of a 10 V dc-biased 300 V ac electric voltage. The curved-line arrows highlight the particles trapped in the bulk fluid by the recirculating flows of ICEO. The block arrow indicates the particle traveling direction. The scale bar represents 50 μm.

In-reservoir electrokinetic preconcentration of *E. coli* cells

The application of the above-demonstrated in-reservoir electrokinetic preconcentration technique in *E. coli* cells is demonstrated in Fig. 6 (see Movie 4 in the ESI†). All working conditions are identical to those in Fig. 5 for 1 μm polystyrene particles. Therefore, the strength of ICEO should remain the same and the effect of DEP on cell preconcentration should be still minor. Indeed, strong fluid vortices occur immediately after the electric field is switched on, which quickly wrap and

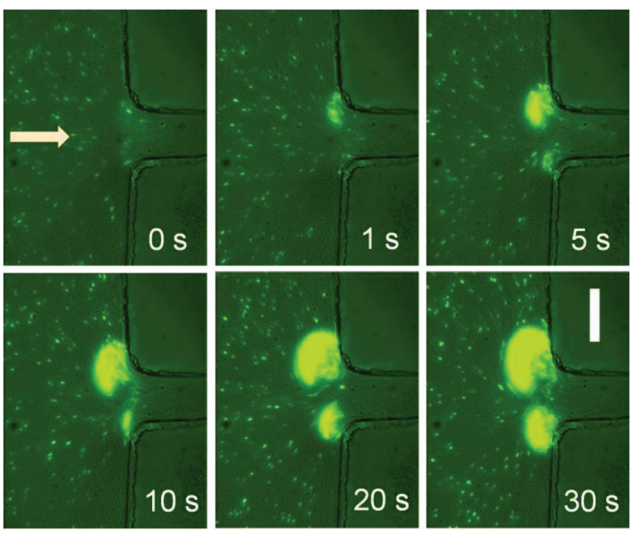

Fig. 6 Time development of in-reservoir electrokinetic preconcentration of fluorescently stained *E. coli* cells under 10 V dc-biased 300 V ac. The constricted section of the microchannel (see Fig. 1) is 50 μm wide. The block arrow indicates the cell traveling direction. The scale bar represents 50 μm.

preconcentrate cells near the two corners (see the images within the first 5 s in Fig. 6). Even after they have been greatly concentrated with significantly expanded and enhanced fluorescence signals (see images after 5 s in Fig. 6), the cells are still trapped completely inside the reservoir. Moreover, no cells are observed to trap onto the channel walls of the two corners by positive DEP during the course of the test. The average *E. coli* cell concentration in the two vortices after 30 s was estimated using ImageJ software (Wayne Rasband, National Institute of Health) and found to be at least 15 times greater than that prior to pre-concentration. The observed uneven cell distribution in the two vortices may be due to the slight asymmetry of the two corners which is a consequence of the fabrication defect. It is important to note that live *E. coli* cells might actually experience negative DEP in the test because the electric conductivity of their membranes has been reported to be of the order 1 nS cm^{-1} (ref. 65) and is hence smaller than that of the suspending medium with σ_m = 6 μS cm^{-1}. This reversed dielectrophoretic motion even if true, however, does not seem to significantly affect the electrokinetic concentration of cells as shown in Fig. 6.

Conclusions

We have demonstrated a new method for the electrokinetic preconcentration of particles and cells in microfluidic reservoirs. This method relies primarily on the strong recirculating flows of ICEO to trap particles and cells near the corners of the reservoir–microchannel interface. (Positive) DEP may also play a role, which, however, is minor unless a small constriction of the microchannel is used at high electric fields. Therefore, the method we demonstrate in this work may potentially be used to preconcentrate submicron-sized bacterial pathogens in dilute mediums with a very low electric conductivity (*e.g.*, water). Moreover, it can be easily implemented in a parallel mode to increase the flow throughput *via*, for example, a radial arrangement of multiple microchannels in a stacked device. As electrokinetic preconcentration takes place inside the reservoir, the necessary transport of particles and cells from the reservoir to the in-channel analysis region is eliminated. This can save the entire microchannel for post-analysis and greatly simplify device fabrication and operation. We are currently developing a numerical model to predict and understand in-reservoir electrokinetic particle preconcentration. This model will provide the electric field for electrokinetic velocity, $\mathbf{U}_{EK}$, and dielectrophoretic velocity, $\mathbf{U}_{DEP}$, of particles, the flow field for ICEO velocity, $\mathbf{U}_{ICEO}$, of the suspending medium, and the concentration field for the trapped particles.

Acknowledgements

This work was supported in part by Clemson University through the Honors Undergraduate Research Program and the Creative Inquiry Program.

References

1 Q. Ramadan and M. A. Gijs, *Microfluid. Nanofluid.*, 2012, **13**, 529–542.
2 Y. Gao, W. Li and D. Pappas, *Analyst*, 2013, **138**, 4714–4721.
3 B. Cetin, M. B. Ozer and M. E. Solmaz, *Biochem. Eng. J.*, 2014, **92**, 63–82.
4 E. D. Pratt, C. Huang, B. G. Hawkins, J. P. Gleghorn and B. J. Kirby, *Chem. Eng. Sci.*, 2011, **66**, 1508–1522.
5 A. Karimi, S. Yazai and A. M. Ardekani, *Biomicrofluidics*, 2013, **7**, 021501.
6 R. M. Johann, *Anal. Bioanal. Chem.*, 2006, **385**, 408–412.
7 J. Nilsson, M. Evander, B. Hammarstrom and T. Laurell, *Anal. Chim. Acta*, 2009, **649**, 141–157.
8 D. Juncker, H. Schmid and E. Delamarche, *Nat. Mater.*, 2005, **4**, 622–628.
9 M. N. Hamblin, J. Xuan, D. Maynes, H. D. Tolley, D. M. Belnap, A. T. Woolley, M. Lee and A. R. Hawkins, *Lab Chip*, 2010, **10**, 173–178.
10 T. F. Didar and M. Tabrizian, *Lab Chip*, 2010, **10**, 3043–3053.
11 J. Shi, D. Ahmed, X. Mao, S. S. Lin and T. J. Huang, *Lab Chip*, 2009, **9**, 2890–2895.
12 B. Hammarström, M. Evander, H. Barbeau, M. Bruzelius, J. Larsson, T. Laurell and J. Nilsson, *Lab Chip*, 2010, **10**, 2251–2257.
13 M. Nordin and T. Laurell, *Lab Chip*, 2012, **12**, 4610–4616.
14 Y. Chen, S. Li, Y. Gu, P. Li, X. Ding, J. P. McCoy, S. J. Levine, L. Wang and T. J. Huang, *Lab Chip*, 2014, **14**, 924–930.
15 S. A. Peyman, E. Y. Kwan, O. Margarson, A. Iles and N. Pamme N, *J. Chromatogr., A*, 2009, **1216**, 9055–9062.
16 M. D. Tarn, S. A. Peyman and N. Pamme, *RSC Adv.*, 2013, **3**, 7209–7214.
17 J. Zeng, C. Chen, P. Vedantam, T. R. Tzeng and X. Xuan, *Microfluid. Nanofluid.*, 2013, **15**, 49–55.
18 J. J. Wilbanks, G. Kiessling, J. Zeng, C. Zhang and X. Xuan, *J. Appl. Phys.*, 2014, **115**, 044907.
19 S. J. Williams, A. Kumar and S. T. Wereley, *Lab Chip*, 2008, **8**, 1879–1882.
20 Y. Zhang, H. Lei, Y. Li and B. Li, *Lab Chip*, 2012, **12**, 1302–1308.
21 A. Kayani, K. Khoshmanesh, S. A. Ward, A. Mitchell and K. Kalantar-zadeh, *Biomicrofluidics*, 2012, **6**, 031501.
22 C. Zhao, Y. Xie, Z. Mao, Y. Zhao, J. Rufo, S. Yang, F. Guo, J. D. Mai and T. J. Huang, *Lab Chip*, 2014, **14**, 384–391.
23 O. D. Velev and K. H. Bhatt, *Soft Matter*, 2006, **2**, 738–750.
24 J. Voldman, *Annu. Rev. Biomed. Eng.*, 2006, **8**, 425–454.
25 Y. Kang and D. Li, *Microfluid. Nanofluid.*, 2009, **6**, 431–460.
26 M. Kim, M. Jia and T. Kim, *Analyst*, 2013, **138**, 1370–1378.
27 M. Kim and T. Kim, *Analyst*, 2013, **138**, 6007–6015.
28 G. L. Lettieri, A. Dodge, G. Boer, N. F. de Rooij and E. Verpoorte, *Lab Chip*, 2003, **3**, 34–39.
29 P. K. Wong, C. Y. Chan, T. H. Wang and C. M. Ho, *Anal. Chem.*, 2004, **76**, 6908–6914.
30 J. Wu, Y. X. Ben and H. C. Chang, *Microfluid. Nanofluid.*, 2005, **2**, 161–167.

31 S. E. Yalcin, A. Sharma, S. Qian, S. W. Joo and O. Baysal, *Electrophoresis*, 2010, **31**, 3711–3718.
32 T. M. Squires and M. Z. Bazant, *J. Fluid Mech.*, 2004, **509**, 217–252.
33 S. K. Thamida and H.-C. Chang, *Phys. Fluids*, 2002, **14**, 4315.
34 J. K. Chen and R. J. Yang, *Microfluid. Nanofluid.*, 2008, **5**, 719–725.
35 M. Zehavi and G. Yossifon, *Phys. Fluids*, 2014, **26**, 082002.
36 M. Lian, N. Islam and J. Wu, *J. Nanobiotechnol.*, 2007, **1**, 36–43.
37 J. Oh, R. Hart, J. Capurro and H. Noh, *Lab Chip*, 2009, **9**, 62–78.
38 R. Pethig, *Biomicrofluidics*, 2010, **4**, 022811.
39 B. Cetin and D. Li, *Electrophoresis*, 2009, **30**, 3124–3133.
40 B. H. Lapizco-Encinas and M. Rito-Palmomares, *Electrophoresis*, 2007, **28**, 4521–4538.
41 C. Zhang, K. Khoshmanesh, A. Mitchell and K. Kalantar-zadeh, *Anal. Bioanal. Chem.*, 2010, **396**, 401–420.
42 M. Li, W. Li, J. Zhang, G. Alici and W. Wen, *J. Phys. D: Appl. Phys.*, 2014, **47**, 063001.
43 H. Shafiee, J. L. Caldwell, M. B. Sano and R. D. Davalos, *Biomed Microdevices*, 2009, **11**, 997–1006.
44 S. K. Srivastava, A. Gencoglu and A. R. Minerick, *Anal. Bioanal. Chem.*, 2010, **399**, 301–321.
45 J. Regtmeier, R. Eichhorn, M. Viefhues, L. Bogunovic and D. Anselmetti, *Electrophoresis*, 2011, **32**, 2253–2273.
46 B. H. Lapizco-Encinas, B. A. Simmons, E. B. Cummings and Y. Fintschenko, *Electrophoresis*, 2004, **25**, 1695–1704.
47 B. G. Hawkins, A. E. SmithE, Y. A. Syed and B. J. Kirby, *Anal. Chem.*, 2007, **79**, 7291–7300.
48 M. D. Pysher and M. A. Hayes, *Anal. Chem.*, 2007, **79**, 4552–4557.
49 C. Church, J. Zhu, G. Huang, T. R. Tzeng and X. Xuan, *Biomicrofluidics*, 2010, **4**, 044101.
50 N. Lewpiriyawong, C. Yang and Y. C. Lam, *Microfluid. Nanofluid.*, 2012, **12**, 723–733.
51 W. A. Braff, A. Pignier and C. R. Buie, *Lab Chip*, 2012, **12**, 1327–1331.
52 I. F. Cheng, S. C. Chiang, C. C. Chung, T. M. Yeh and H. C. Chang, *Biomicrofluidics*, 2014, **8**, 061102.
53 S. Patel, D. Showers, P. Vedantam, T. R. Tzeng, S. Qian and X. Xuan, *Biomicrofluidics*, 2012, **6**, 034102.
54 S. Patel, S. Qian and X. Xuan, *Electrophoresis*, 2013, **34**, 961–968.
55 J. Zhu, G. Hu and X. Xuan, *Electrophoresis*, 2012, **33**, 916–922.
56 A. Kale, S. Patel, S. Qian, G. Hu and X. Xuan, *Electrophoresis*, 2014, **35**, 721–772.
57 D. Yan, C. Yang and X. Huang, *Microfluid. Nanofluid.*, 2007, **3**, 333–340.
58 J. Sambrook and D. W. Russell, *Molecular cloning: a laboratory manual*, Cold Spring Harbor Laboratory Press, Cold Spring Harbor, 3rd edn, 2001.
59 X. Xuan, *Electrophoresis*, 2008, **29**, 33–43.
60 C. Zhao and C. Yang, *Phys. Rev. E: Stat. Phys., Plasmas, Fluids, Relat. Interdiscip. Top.*, 2011, **83**, 066304.
61 C. Zhao and C. Yang, *Electrophoresis*, 2011, **32**, 629–637.
62 G. Yossifon, I. Frankel and T. Miloh, *Phys. Fluids*, 2006, **18**, 117108.
63 Y. Eckstein, G. Yossifon, A. Seifert and T. Miloh, *J. Colloid Interface Sci.*, 2009, **338**, 243–249.
64 I. Ermolina and H. Morgan, *J. Colloid Interface Sci.*, 2005, **285**, 419–428.
65 B. H. Lapizco-Encinas, B. A. Simmons, E. B. Cummings and Y. Fintschenko, *Anal. Chem.*, 2004, **76**, 1571–1579.